Preprints of the 21st IFAC World Congress (Virtual)
Berlin, Germany, July 12-17, 2020

Modeling and Control of a Thermoelectric Structure with a Peltier Element Subject to External Disturbances ⋆

Alexander Gavrikov * **Georgy Kostin** * **Harald Aschemann** ** **Andreas Rauh** **

* *Ishlinsky Institute for Problems in Mechanics RAS, Moscow, Russia (e-mail: {gavrikov, kostin}@ipmnet.ru).*
** *Chair of Mechatronics, University of Rostock, Justus-von-Liebig Weg 6, D-18059 Rostock, Germany (e-mail: {Harald.Aschemann, Andreas.Rauh}@uni-rostock.de).*

Abstract: A nonlinear model of heat transfer in a solid structure controlled by a Peltier element is considered. The thermoelectrical converter in between two cylindrical bodies regulates temperature distribution in one cylinder, while the other body is used as the thermal capacitor. An optimal control problem is stated to minimize heat losses in the electrical circuit of the Peltier element in a given time interval. A feedforward piecewise constant control signal is designed to reach the vicinity of a desired steady state by using the a-priori prediction of variations of the external temperature. Additionally, feedback loops are designed for model linearization, trajectory stabilization, and compensation of changes in the ambient air temperature.

Keywords: Nonlinear control systems, partial differential equations, feedback linearization and stabilization, feedforward control, parameter optimization, Peltier element

1. INTRODUCTION

The control of heat transfer in solid structures sometimes employs well-known physical phenomena but involves original implementation. In this paper, a nonlinear model of processes in thermally conductive bodies controlled by a thermoelectric converter is considered. In such control elements, flow of electric charge influenced by electromotive force can transfer a part of thermal energy from colder area to the hotter one, Goupil et al. (2011). The phenomenon is based on the effect stated by J. Peltier. And vice versa, temperature differences cause electric currents according to the Seebeck effect. The reliable modeling of such processes is important for design and optimization of precise control laws. Thus, a set of interrelated phenomena, such as recuperation of heat flux into electric energy, thermal conductivity of semiconductor material, Joule heat losses, and heat exchange between the system and the environment, have to be taken into account. These phenomena are often ignored or simplified in control problems, Chavez et al. (2000). Frequently, only one-dimensional models are used or the steady-state case is supposed, Cernaianu and Gontean (2013). Not rare, a system with lumped parameters is applied for control design, Felgner et al. (2014).

In our previous studies, simplified thermoelectrical models of heat transfer in solids were considered and control strategies for them were constructed, see Kostin et al. (2018) and Gavrikov and Kostin (2018). The nonlinear model for a structure controlled by a Peltier element (PE) was proposed, steady state solutions were studied in Kostin et al. (2019), the model was verified in Gavrikov et al. (2019a) as well as in Knyazkov et al. (2019), and feedforward control with feedback linearization was proposed in Gavrikov et al. (2019b).

In the current paper, the previous feedforward control laws are modified and enhanced by accounting for external disturbances, namely, the varying ambient temperature. Such a modification is a necessary feature for the experimental validation of possible control strategies. A new feedforward control law exploiting the a-priori prediction of the ambient temperature is proposed. The linearization with respect to internal and external temperatures in the vicinity of the feedforward control trajectory is used to design a feedback control consisting of two loops. One aims at the stabilizing the temperatures along the feedforward trajectory, whereas the other suppresses the mean value of the disturbance. As a result, the composed control law is a sum of four components: the feedback linearization signal, the feedforward piecewise constant control, the stabilizing feedback signal, and the compensating feedback term.

2. THERMOELECTRIC MODEL OF THE PELTIER ELEMENT FOR THE CYLINDRICAL STRUCTURE

In our study, the following experimental setup constructed at the Chair of Mechatronics of the University of Rostock, Germany, is considered. It consists of two identical aluminum cylinders arranged vertically with a PE located in between them, see Fig. 1. The overall structure is thermally insulated on the top and bottom surfaces. On its lateral surface, heat transfer w.r.t. the ambient air

⋆ The study was financially supported partly by the Russian Foundation for Basic Research (19-01-00173), and the RAS Presidium (program AAAA-A17-117121120031-8), Russia.

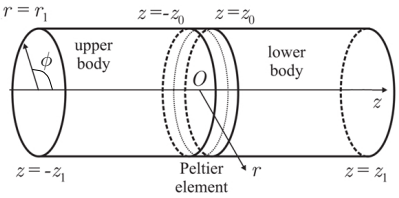

Fig. 1. Schematic representation of the experimental setup.

takes place. The PE is supplied with the chosen input voltage, and the temperature is measured by means of PT100 resistance sensors on the surface of the cylinders. The ambient temperature, which is changing during the experiment, is measured at several points near the setup.

The physical parameters for the cylinders and the PE have been determined in Rauh et al. (2015), Kostin et al. (2019), Gavrikov et al. (2019a), Knyazkov et al. (2019). For the cylinders, the parameters are as follows: the thermal conductivity $\lambda_a = 254.4$ W/m/K, the density $\rho_a = 2700$ kg/m^3, the specific heat capacity $c_a = 896$ J/kg/K, the height $h = 0.1$ m, the radius $r_1 = 0.031$ m. As for the PE, its parameters are: $\lambda_p = 0.517$ W/m/K, $\rho_p = 300$ kg/m^3, $c_p = 500$ J/kg/K, the height $z_0 = 0.00195$ m; its radius is identical to the one of the cylinders, the Seebeck coefficient $S = 0.0427$ W/K/A and the resistance $R = 6.03\ \Omega$. The electrical control circuit is characterized by the threshold voltages $u_+ = 1.115$ V and $u_- = -1.29$ V. Addressing the convective heat exchange on the circumferential surface, the heat transfer coefficient α is given by 8.4 W/m^2/K. The volume of the PE is $|\mathcal{V}_p| = 2\pi r_1^2 z_0$, and its cross-section area is $\mathcal{A}_p = \pi r_1^2$.

Taking into account only the integral behavior of the PE, we assume that

- the heat exchange of the PE with the surrounding air is negligibly small;
- the inner structure of the PE is homogeneously transversal isotropic with respect to both electrical and thermal conductivities;
- the conductivity coefficient along the z-axis is much larger than those along the other axes, as the PE is oriented in the z direction, see Fig. 1;
- the Seebeck coefficient is constant as a general characteristic of the thermoelectric properties.

According to the design of the experimental setup, the cylindrical coordinates are utilized further: $\mathbf{x} = (r, \phi, z)$. The corresponding domains are defined as $\mathcal{V}_p = I_r \times I_\pi \times I_p$ for the PE and $V_k = I_r \times I_\pi \times I_k$ for the upper ($k = 1$) and lower ($k = 2$) cylinders. Here, $I_r = [0, r_1]$, $I_\pi = [0, 2\pi]$, $I_p = [-z_0, z_0]$, $I_1 = [z_0, z_1]$, $I_2 = [-z_1, -z_0]$. Let us denote the temperature relative w.r.t. θ^0 as $\theta(t, \mathbf{x})$, the electric current as $J(t)$ and the control voltage as $U(t)$. Then, the following nonlinear model was validated in Kostin et al. (2019), Gavrikov et al. (2019a), Knyazkov et al. (2019):

$$c_p\rho_p\dot\theta = \lambda_p\theta''_{zz} + \frac{RJ^2(U,\theta)}{|\mathcal{V}_p|}, \quad \mathbf{x}\in\mathcal{V}_p, \tag{1}$$

$$c_a\rho_a\dot\theta = \lambda_a\Delta\theta, \quad \mathbf{x}\in\mathcal{V}_k, \quad k = 1,2, \tag{2}$$

$$\theta'_z|_{|z|=z_1} = 0, \quad \alpha\theta + \lambda_a\theta'_r|_{r=r_1,|z|>z_0} = \alpha\theta_A, \tag{3}$$

$$\theta|_{|z|=z_0\pm0} = \theta|_{|z|=z_0\mp0}, \tag{4}$$

$$-\lambda_a\theta'_z|_{|z|=z_0+0} = \left[(\theta+\theta^0)\frac{SJ(U,\theta)}{\mathcal{A}_p} - \lambda_p\theta'_z\right]_{|z|=z_0-0} \tag{5}$$

with the initial condition $\theta(0, \mathbf{x}) = \Theta(\mathbf{x})$. In the first heat equation (1), the quadratic term w.r.t. the current J corresponds to the Joule heating of the PE. The second heat equation (2) describes the usual heat transfer in the cylinders. The first equation in (3) corresponds to the insulation on the cylinders' ends and the last equation reflects the heat exchange with the ambient air. The forth and the fifth lines (4), (5) define the continuity of the temperature and the heat flux, respectively, whereas the term in (5) with the current J reflects the heat flux generated due to the Peltier effect.

In practical implementations of thermoelectric converters, the input voltage often has threshold levels. Thus, the voltage provided to the PE is supposed to be equal to

$$RJ = RJ(U,\theta) = \begin{cases} \mathcal{E} - u_-, & \mathcal{E} < u_-, \\ 0, & u_- \le \mathcal{E} \le u_+, \\ \mathcal{E} - u_+, & \mathcal{E} > u_+, \end{cases} \tag{6}$$

where $\mathcal{E} = U - S[\tilde\theta]$ is the electromotive force, $u_\pm$ are the threshold voltages, $\tilde\theta$ is the mean temperature averaged over its cross-section, and the square brackets denote the jump of the temperature between the top and bottom surfaces of the PE: $[\tilde\theta] = \tilde\theta|_{z=z_0} - \tilde\theta|_{z=-z_0}$.

3. FEEDBACK LINEARIZATION AND MODEL-ORDER REDUCTION

The considered system contains terms nonlinear w.r.t. both the control voltage and the temperature distribution. To simplify the problem (1)–(6), the following feedback control

$$U = u_0 + U_f, \quad U_f = S[\tilde\theta] \tag{7}$$

is introduced, see Gavrikov et al. (2019b). Then, we obtain an initial-boundary value problem (IBVP)

$$\begin{gathered} c_p\rho_p\dot\theta = \lambda_p\theta''_{zz} + \frac{u^2}{R|\mathcal{V}_p|}, \quad \mathbf{x}\in\mathcal{V}_p, \\ c_a\rho_a\dot\theta = \lambda_a\Delta\theta, \quad \mathbf{x}\in\mathcal{V}_k, \quad k = 1,2, \\ \theta'_z|_{|z|=z_1} = 0, \quad \alpha\theta + \lambda_a\theta'_r|_{r=r_1,|z|>z_0} = \alpha\theta_A, \\ \theta|_{|z|=z_0\pm0} = \theta|_{|z|=z_0\mp0}, \\ -\lambda_a\theta'_z|_{|z|=z_0+0} = \left[(\theta+\theta^0)\frac{Su}{R\mathcal{A}_p} - \lambda_p\theta'_z\right]_{|z|=z_0-0}, \\ \theta(0,\mathbf{x}) = \Theta(\mathbf{x}), \\ u(t) = \begin{cases} u_0(t) - u_- & \text{for} \quad u_0 < u_- \\ 0 & \text{for} \quad u_- \le u_0 \le u_+ \\ u_0(t) - u_+ & \text{for} \quad u_0 > u_+ \end{cases}. \end{gathered} \tag{8}$$

3.1 Separation of variables for model order reduction

Although the problem (8) is still nonlinear w.r.t. the control input, it is possible to analyze it explicitly by using some simplifications. Due to linearity of the problem (8) w.r.t. the temperature, the Fourier analysis can be implemented for a constant control function u. Note that, in this case, the overall control signal U according to (7) is non-constant and still depends on the temperature because of the component U_f. In what follows, the ansatz functions

$$\Theta = e^{\nu t}\Xi(r,\phi,z), \ \Xi(r,\phi,z) = J_n(\mu r/r_1)\cos(n\phi)\psi(z), \tag{9}$$

with $n = 0, 1, \ldots,$ are utilized to obtain an analytical solution. Here, J_n is the Bessel function of the first kind of the order n. The substitution of (9) into (8) leads to the corresponding eigenproblem

$$\begin{gathered}\psi'' = -\frac{\xi^2}{r_1^2}\psi,\ z \in Z_a^{\pm}; \quad \psi'' = \frac{\nu c_p \rho_p}{\lambda_p}\psi,\ z \in Z_p; \\ \psi'(-z_1) = \psi'(z_1) = 0,\ \psi(\pm z_0 + 0) = \psi(\pm z_0 - 0), \\ \lambda_a \psi'|_{z=\pm z_0 \pm 0} = \left[\lambda_p \psi' - \frac{Su\psi}{R\mathcal{A}_p}\right]_{z=\pm z_0 \mp 0},\end{gathered} \tag{10}$$

where $\psi = \psi_{n,m,k}$ are eigenfunctions (EFs), $\xi = \xi_{n,m,k}$ are the eigenvalues (EVs) w.r.t the z variable, and

$$\nu(\xi) = \nu_{n,m,k} = -\frac{\lambda_a(\mu^2 + \xi^2)}{c_a \rho_a r_1^2} \tag{11}$$

denotes the EVs w.r.t. time with $n, m, k \in \{0, 1 \ldots\}$. The EVs w.r.t. the radial axis $\mu = \mu_{n,m}$ are consecutive positive roots of the equation

$$\alpha J_n(\mu) + \frac{\lambda_a}{r_1}(nJ_n(\mu) - \mu J_{n+1}(\mu)) = 0. \tag{12}$$

The solution of (10) is found explicitly using the piecewise-defined EFs

$$\psi(z) = \begin{cases} \psi_{\pm}(z) & \text{for} \quad z \in Z_a^{\pm}, \\ \psi_P(z) & \text{for} \quad z \in Z_p, \end{cases} \tag{13}$$

with $\psi_{\pm,P}$ taken as combinations of trigonometric and exponential functions, see Gavrikov et al. (2019b).

These EFs are orthogonal w.r.t. the following dot product

$$(w, v) = \int_{I_1 \cup I_2} c_a \rho_a w(z) v(z) dz + \int_{I_p} c_p \rho_p w(z) v(z) dz, \tag{14}$$

which is used further for all the expansions involved.

It is worth noting that the EFs ψ depend here on the control u. Nevertheless, due to simplicity of the involved computations, these EFs can be used for the solution of the problem for any given $u(t)$ at the current time instant.

3.2 Approximation of a steady-state solution

Similarly, the steady-state solution for the problem (8) is obtained by using the ansatz functions Ξ and taking $\dot{\theta} = 0$. The corresponding boundary value problem for $\theta_A = 0$ is

$$\begin{gathered}\psi'' = \frac{\mu^2}{r_1^2}\psi,\ z \in Z_a^{\pm}; \quad \psi'' = \frac{\omega_1}{\lambda_p}\frac{u^2}{R|\mathcal{V}_p|},\ z \in Z_p; \\ \psi'(-z_1) = \psi'(z_1) = 0, \quad \psi(\pm z_0 + 0) = \psi(\pm z_0 - 0), \\ \lambda_a \psi'|_{z=\pm z_0 \pm 0} = \left[\lambda_p \psi' - \frac{Su\psi}{R\mathcal{A}_p} - \frac{\omega_1 S\theta^0 u}{R\mathcal{A}_p}\right]_{z=\pm z_0 \mp 0}.\end{gathered} \tag{15}$$

Its solution is found in a standard way by the method of undetermined coefficients by employing

$$\begin{gathered}\psi_{\pm}(z) = C_{1,2}\cos(\mu(z \mp z_1)/r_1), \\ \psi_P(z) = C_3 + C_4 z + z^2 \frac{\omega_1}{2\lambda_p}\frac{u^2}{R|\mathcal{V}_p|},\ \omega_1 = \frac{(\int_0^{r_1} rJ_n dr)}{\int_0^{r_1} rJ_n^2 dr}.\end{gathered} \tag{16}$$

Further, we consider a non-zero ambient temperature θ_A. In this case, the temperature distribution has the same shape but is shifted up to the value θ_A. The constants C_1, C_2, C_3 in (16) are calculated by taking $\theta^0 + \theta_A$ instead of θ^0 in (15).

The analytical representation of the steady state solution involves the expansion w.r.t. the obtained EFs. However, we consider further only its four-modes approximation related to $\mu_{0,0}$. The significance of the lowest EVs w.r.t. to the radial axis $\mu_{0,0}$ is discussed in Kostin et al. (2019), Gavrikov et al. (2019a), Gavrikov et al. (2019b). It turns out that only the four lowest eigenmodes with $m = n = 0$, $k = 0, \ldots, 3$ are sufficient for modeling on time intervals greater than several seconds. That can be illustrated by a comparison of the characteristic times $\tau = \tau_{n,m,k}$ (inverse of decay rates ν) for several lowest eigenmodes given in Table 1 for $u = 1$ V (first row) and $u = 20$ V (second row). Also, it is worth mentioning that the shape of the EFs does not change significantly with the change of the input voltage except for the zeroth eigenmode.

4. FEEDFORWARD CONTROL

In this section, feedback linearization is utilized for a simplification and the subsequent design of feedforward control.

4.1 Modal representation with four ODEs

Having in mind the previous remarks on the EFs, we restrict ourselves to the case $m = n = 0$, $k = 0, \ldots, 3$ and expand the solution of the problem (8) as

$$\theta(t, r, \phi, z) = \sum\nolimits_{k=0}^{3} \theta_{0,0,k}(t) J_0(\mu_{0,0} r/r_1) \psi_{0,0,k}(z). \tag{17}$$

After substituting (17) into (8) and projecting the results onto the EFs, the following ODE system is obtained (the zeroth subindices m and n are omitted)

$$\begin{gathered}\dot{\bar{\theta}} = A\bar{\theta} + F(u, \theta_A, \theta^0), \quad \bar{\theta}(0, z) = \bar{\Theta}, \\ \bar{\theta} = (\theta_0, \ldots, \theta_3)^T, \quad \bar{\Theta} = (\Theta_0, \ldots, \Theta_3)^T, \\ \Theta_i = \int_{\mathcal{V}} \Theta(\bar{x}) \Xi_i(\bar{x}) d\bar{x}, \quad \Xi_i = J_0\left(\mu_{0,0} r/r_1\right) \psi_{0,0,i}\end{gathered} \tag{18}$$

Here, $\mathcal{V} = \mathcal{V}_p \cup \mathcal{V}_1 \cup \mathcal{V}_2$, the diagonal (due to the orthogonality of the EFs) matrix $A = \mathrm{diag}(\nu_0, \ldots, \nu_3)$ and the vector $F = (F_0, \ldots, F_3)^T$ are introduced with

$$\begin{aligned}F_i = \frac{u^2 \omega_1}{R|\mathcal{V}_p|}\int_{I_p} \psi_i dz + \frac{Su\theta^0\omega_1}{R\mathcal{A}_p}[\psi_i] + \\ \frac{\alpha\theta_A r_1 J_0(\mu_{0,0})}{\int_0^{r_1} rJ_0^2 dr}\int_{I_1 \cup I_2} \psi_i dz,\end{aligned}$$

where the ambient temperature θ_A is supposed to be constant w.r.t. spatial variables.

4.2 Piecewise constant control processes

Suppose that the predicted ambient temperature θ_p has an analytical expression (e.g., polynomial). Then, the

Table 1. Characteristic times in sec.

$\tau_{0,0,0}$	$\tau_{0,0,1}$	$\tau_{0,0,2}$	$\tau_{0,0,3}$	$\tau_{0,0,4}$	$\tau_{1,0,0}$	$\tau_{0,1,0}$
4467	778.6	9.61	9.42	2.41	0.62	2.69
5248	760.2	9.62	9.41	2.41	0.62	2.69

ODE system (18) can be solved for any given constant u explicitly. If $u(t)$ is a piecewise step function with values u_i, $i = 0, \dots, N$ and switching instants T_i, then (18) can be solved on each time interval $[T_i, T_{i+1}]$ by using the matrix A and the vector F that correspond to the EFs obtained for the current value u_i.

At the switching instants T_i, the current temperature distribution $\theta = \sum \theta_j \psi_j^{(i-1)}$ should be re-expanded w.r.t. the new EFs: $\theta = \sum \theta_j \psi_j^{(i)}$, and the new values $\bar{\Theta}_i$ of $\theta(T_i)$ serve as initial conditions for the system (18).

In such a way, we can calculate analytically the distribution and the behavior of the temperature w.r.t. time for any given piecewise step function $u(t)$ and the predicted ambient temperature $\theta_p(t)$.

4.3 Terminal temperature distribution

As an objective, we consider an approximate steady-state solution θ_{st} of (8) obtained by means of (15). However, any steady state depends on the input voltage and the ambient temperature as parameters. We aim at a steady-state solution that has a prescribed average temperature θ_{av} in the upper cylinder

$$\Big(\frac{1}{\mathcal{V}_1}\int_{\mathcal{V}_1} \theta_{st} dV - \theta_{av}\Big)^2 \to \min_u \tag{19}$$

for a given (predicted) behavior of the ambient temperature $\theta_p(t)$. Thus, the lower cylinder is considered as a heat capacitor and the upper one as the controlled subsystem.

The minimization problem (19) is solved explicitly because the dependence of a steady-state solution on the control voltage u is available according to Sec. 3.2.

4.4 Optimal feedforward control

Let us consider the following cost function

$$\Phi = \frac{\gamma_u}{T}\int_0^T u^2(t)dt + \frac{\gamma_\theta}{|\mathcal{V}|}\|\theta|_{t=T} - \theta_{st}\|^2_{L_2}, \tag{20}$$

where θ_{st} is the solution of (19). The optimal control problem

$$\Phi[u, \theta] \to \min_u \tag{21}$$

for some fixed T can be solved numerically by applying the gradient descent method. For simplicity, we suppose that $u(t)$ is sought in the space of piecewise step functions defined on $[0, T]$ with switches at $T_i = iT/4$, $i = 1, 2, 3$: $u(t) = u_{FF}(t) = \{u_{FF0}, u_{FF1}, u_{FF2}, u_{FF3}\}$. We consider 4 switches since such a choice allows to transfer a linear 4-mode system into the desired state, although this is not guaranteed in the studied nonlinear case. Since u_{FFk}, $(k = 0, \dots, 3)$ are constants, the corresponding temperature behavior θ_{FF} is calculated analytically according to Sec. 4.2. Therefore, each iteration of the gradient descent method is also executed analytically, which guarantees the fast performance of the method's steps.

5. FEEDBACK COMPENSATION OF AMBIENT TEMPERATURE DISTURBANCES

Although the feedforward control law allows to reach a vicinity of the desirable state, the resulting accuracy can be affected by undesirable disturbances. For the studied experimental setup, the ambient temperature $\theta_A(t)$ serves as such a disturbance, which can vary up to several degrees during the test. Thus, its compensation should be provided by the controller.

At first, let us denote the feedforward control law and the corresponding temperature distribution according to Sec. 4.4 as $u_{FF}(t)$ and $\theta_{FF}(t, \mathbf{x})$, respectively. Suppose that the ambient temperature $\theta_A(t)$ deviates from the predicted value $\theta_p(t)$ by a small value $\delta\theta_A(t) : \theta_A = \theta_p + \delta\theta_A$, $\|\delta\theta_A\| \ll \|\theta_p\|$. We assume that $\theta_p(t)$ is given a priori and not estimated during the process. Then, the overall control voltage is decomposed into the following parts

$$U = u_0 + U_f, \quad U_f = S[\tilde{\theta}], \quad u_0 = u_{FF} + v \pm u_\pm, \tag{22}$$

where v corresponds to the compensation of the ambient temperature. The related temperature distribution is represented as

$$\theta = \theta_{FF} + y, \quad \|y\| \ll \|\theta_{FF}\|. \tag{23}$$

Now, the IBVP (8) is linearized w.r.t. u_{FF}, θ_{FF} and θ_p :

$$\begin{gathered} c_p\rho_p\dot{y} = \lambda_p y''_{zz} + \frac{2u_{FF}v}{R|\mathcal{V}_p|}, \quad \mathbf{x} \in \mathcal{V}_p, \\ c_a\rho_a\dot{y} = \lambda_a\Delta y, \quad \mathbf{x} \in V_k, \quad k = 1, 2, \\ y'_z|_{|z|=z_1} = 0, \quad \alpha y + \lambda_a y'_r|_{r=r_1, |z|>z_0} = \alpha\delta\theta_A, \\ y|_{|z|=\pm z_0 \pm 0} = y|_{|z|=\pm z_0 \mp 0}, \quad -\lambda_a y'_z|_{|z|=z_0+0} = \\ \left[(\theta_{FF} + \theta^0)\frac{Sv}{R\mathcal{A}_p} + \frac{Su_{FF}y}{R\mathcal{A}_p} - \lambda_p y'_z\right]_{|z|=z_0-0}, \\ y(0, \mathbf{x}) = 0. \end{gathered} \tag{24}$$

Note that these equations have the same structure as (8). Thus, the corresponding eigenproblems for (24) and (8) coincide if $u = u_{FF}$ in (10). Therefore, we use the same EFs ψ and EVs ν for the expansion of the solution of (24) that are utilized for finding u_{FF} (see Sec. 4)

$$y = J_0(\mu_{0,0}r/r_1)\sum\nolimits_{i=0}^{3} y_i(t)\psi_i(z). \tag{25}$$

By taking the integral form of (24) and projecting on the EFs, the following ODE system is obtained

$$\dot{\bar{y}} = B\bar{y} + bv + f\delta\theta_A. \tag{26}$$

Here, the vectors and matrices are given by

$$\begin{gathered} \bar{y} = (y_0, \dots, y_3)^T, \ B = A + C, \ A = \mathrm{diag}(\nu_0, \dots, \nu_3), \\ C_{ij} = -\frac{Su_{FF}}{R\mathcal{A}_p}[\psi_i\psi_j], \quad f_i = \frac{\alpha r_1 J_0(\mu_{0,0})}{\int_0^{r_1} rJ_0^2 dr}\int_{I_1\cup I_2}\psi_i dz, \\ b_i = \frac{2u_{FF}\omega_1}{R|\mathcal{V}_p|}\int_{I_p}\psi_i dz + \frac{S\theta^0}{R\mathcal{A}_p}[\psi_i] + \frac{S}{R\mathcal{A}_p}[\theta_{FF}\psi_i], \\ b = (b_0, \dots, b_3)^T, \quad f = (f_0, \dots, f_3)^T. \end{gathered}$$

Since we are interested in reaching the state with a certain average temperature, let us introduce a new variable $\tilde{y}(t)$

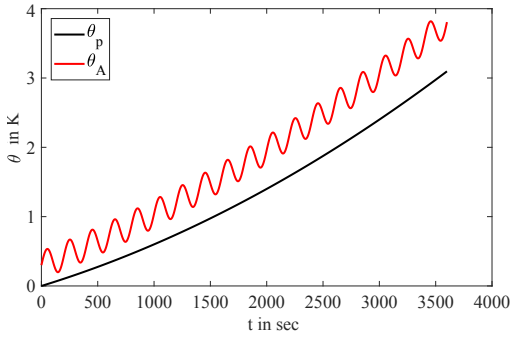

Fig. 2. Predicted vs. real behavior of the ambient temperature.

which characterizes the variation of the average value of the temperature in the upper cylinder

$$\tilde{y} = \sum_{i=0}^{3} a_i y_i(t), \quad a_i = \frac{1}{\mathcal{V}_1} \int_{\mathcal{V}_1} J_0 \psi_i dV. \tag{27}$$

After averaging (26) according to (27) with the weights a_i, the following ODE is obtained

$$\dot{\tilde{y}} = a^T A \bar{y} + a^T b v + a^T f \delta\theta_A, \quad a = (a_0, \ldots, a_3)^T, \tag{28}$$

where the ODE (28) should be controllable, i.e., $a^T b \neq 0$.

Now, the control function v is split into two parts

$$v = v_c + v_{FB},$$

where v_c is should compensate for the deviation of the ambient temperature from the predicted value, and v_{FB} should counteract other possible disturbances. Given $\dot{\tilde{y}} = 0$ in (28), the compensating feedback control results in

$$v_c = -\frac{1}{a^T b} \left(a^T A \bar{y} + a^T f \delta\theta_A \right). \tag{29}$$

The additional feedback is taken as

$$v_{FB} = \frac{\kappa}{a^T b} \tilde{y}, \quad \kappa < 0, \tag{30}$$

where $\kappa \sim \nu_1/2$. This choice keeps the transient phase shorter than the interval between control jumps and prevents from exciting the highest modes.

Note that the implementation of (29) requires an appropriate state and disturbance observer to restore the vector $\bar{y}$ by using the temperature measurements on the cylindrical surface.

6. NUMERICAL RESULTS

In this section, the implementation of the compensating feedback control is simulated and corresponding results are presented.

As an example, suppose that the a-priori prediction of the ambient temperature is given by the polynomial

$$\theta_p(t) = 10^{-7} t^2 + 5 \cdot 10^{-4} t,$$

whereas the unknown real change of this temperature is $\theta_A(t) = 0.9 \cdot 10^{-7} t^2 + 1.3 \cdot 5 \cdot 10^{-4} t + 0.3 + 0.2 \sin(\pi t / 10^2)$, which should be measured or estimated during an experiment, see Fig. 2. Then, $\delta\theta_A$ is the difference between the true and expected ambient temperature, which is exploited to check the robustness of the proposed control law.

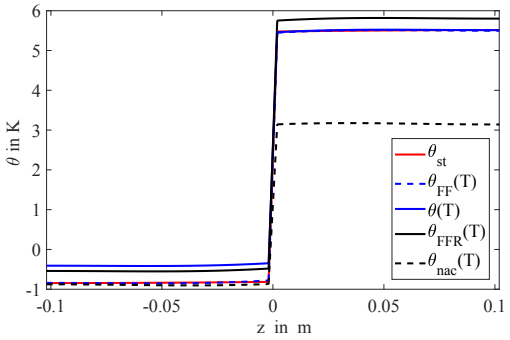

Fig. 3. Distribution of the relative temperature along the z-axis at the terminal time instant T.

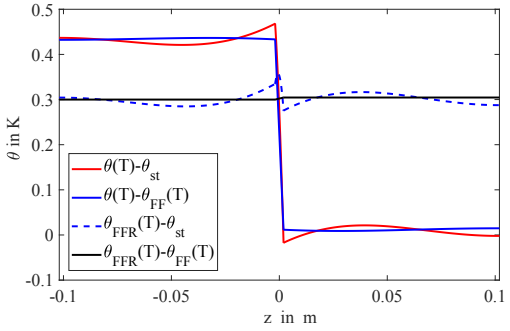

Fig. 4. The differences between terminal temperature distributions.

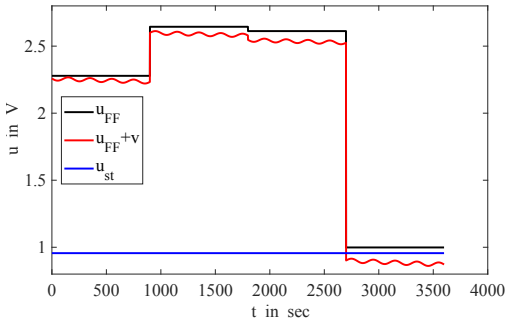

Fig. 5. Comparison of different control actions.

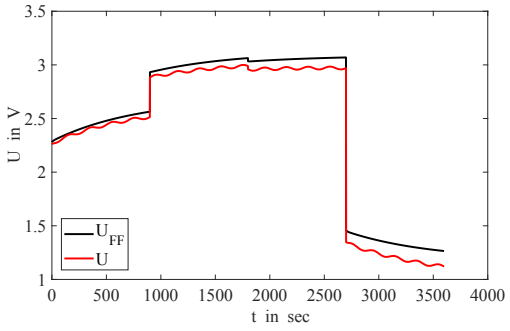

Fig. 6. Voltages provided.

We fix the terminal time instant $T = 1$ h and the desired average temperature in the upper cylinder $\theta_{av} = 5.5$ K. The corresponding approximate steady state θ_{st} is obtained analytically by solving the minimization problem (19). If the related control input $u_{st} \approx 0.96$ V is provided for 1 h, then the resulting distribution $\theta_{nac}(T)$ is rather

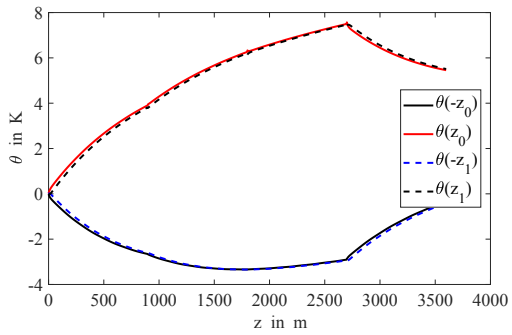

Fig. 7. The behavior of the relative temperatures at the selected points.

distinct from the desired one, see Fig. 3. Here, the predicted behavior of the ambient temperature is supposed.

Next, the time interval $[0, T]$ is divided into four equal parts and the feedforward control u_{FF} law is calculated according to Sec. 4. The corresponding final distribution of the optimized temperature $\theta_{FF}(T)$ is rather close to the desired one θ_{st}, see Fig. 3, where the corresponding curves almost coincide.

However, the real ambient temperature behavior differs from the predicted one. If only the feedforward law is utilized, then the resulting temperature distribution $\theta_{FFR}(T)$ has the form shown in Fig. 3 and the steady-state error $\theta_{FFR}(T) - \theta_{st}$ is depicted in Fig. 4. See also the error $\theta_{FFR}(T) - \theta_{FF}(T)$ there.

Suppose that the compensating feedback signal v is added to the feedforward signal u_{FF}. The resulting distribution $\theta(T)$ is rather close to θ_{st}, see Figs. 3 and 4, although it relates only to the upper cylinder due to the objective of the proposed control as described in Sec. 5, where only the disturbances in the upper cylinder are suppressed.

In Fig. 5, the control actions are shown: the reference signal u_{st} without active control, the feedforward control u_{FF}, and the corrected control input $u_{FF} + v$. According to the proposed feedback linearization, the overall control voltage includes a part that is proportional to the temperature drop on the PE as shown in Fig. 6, where U_{FF} corresponds to u_{FF} and U to $u_{FF} + v$.

The disturbed ODE system (18) is solved numerically on the time interval $[t_n, t_{n+1}]$ with a horizon of 1 sec. The terminal mode amplitudes from the previous step are provided as current initial conditions at t_n. For an experimental implementation, a model-based low-pass filtering can be applied using measurements on the cylinders' surface by, e.g., a Luenberger-type observer, moving-horizon estimation over past measurements, or higher-order sliding mode techniques. The simulated behavior of the temperature at several points is shown in Fig. 7, where the feedback compensation is applied. In the absence of the compensation, the temperature changes similarly, although the influence of the ambient temperature results in gradually growing difference between these cases.

7. CONCLUSIONS AND OUTLOOK

The extension of a feedforward control law, proposed in Gavrikov et al. (2019a), is developed to take into account the long-term a-priori prediction of the ambient temperature. For an effective compensation of such disturbances, an appropriate feedback compensator is designed. The terminal state $\theta(T)$ is close but not equal to the desired steady state θ_{st} with the prescribed average temperature θ_{av}. After the first stage $[0, T]$, the state of the system should be kept as close as possible to a proper steady-state corresponding to θ_{av}. It is possible to use at this stage a prediction of the ambient temperature $\theta_A(t)$, $t > T$, for the calculation of a new control over a fixed horizon. It can be achieved by solving a minimization problem based on the proposed feedback compensator. The next stage of our research will focus on a state and disturbance observer. Moreover, an experimental validation of the overall control strategy at the test rig is planned.

REFERENCES

Cernaianu, M.O. and Gontean, A. (2013). Parasitic elements modelling in thermoelectric modules. *IET Circuits, Devices and Systems*, 7(4), 177–184.

Chavez, J., Ortega, J., Salazar, J., Turo, A., and Garcia, M. (2000). Spice model of thermoelectric elements including thermal effects. In *17th Int. Conf. IMTC 2000*. IEEE, Baltimore.

Felgner, F., Exel, L., Nesarajah, M., and Frey, G. (2014). Component-oriented modeling of thermoelectric devices for energy system design. *IEEE Transactions on Industrial Electronics*, 61(3), 1301–1310.

Gavrikov, A. and Kostin, G. (2018). An integro-differential approach to LQ-optimal control problems for heat transfer in a cylindrical body. In *23rd Int. Conf. MMAR-2018*, 71–76. IEEE, Miedzyzdroje.

Gavrikov, A., Kostin, G., Knyazkov, D., Rauh, A., and Aschemann, H. (2019a). Experimental validation of a nonlinear model for controlled thermoelectric processes in cylindrical bodies. In *24th Int. Conf. MMAR-2019*, 558–563. IEEE, Miedzyzdroje.

Gavrikov, A., Kostin, G., Knyazkov, D., Rauh, A., and Aschemann, H. (2019b). Parameter optimization of control with feedback linearization for a model of thermoelectric processes in cylindrical bodies. In *24th Int. Conf. MMAR-2109*, 342–347. IEEE, Miedzyzdroje.

Goupil, C., Seifert, W., Zabrocki, K., Muller, E., and Snyder, G.J. (2011). Thermodynamics of thermoelectric phenomena and applications. *Entropy*, 13, 1481–1517.

Knyazkov, D., Kostin, G., Gavrikov, A., Aschemann, H., and Rauh, A. (2019). FEM modeling and parameter identification of thermoelectrical processes in cylindrical bodies. In *24th Int. Conf. MMAR-2019*, 501–506. IEEE, Miedzyzdroje.

Kostin, G., Rauh, A., and Aschemann, H. (2018). Modeling, experimental identification, and optimization of heat transfer in a metal bar controlled by Peltier elements. *IFAC-PapersOnLine*, 51(2), 313 – 318.

Kostin, G.V., Rauh, A., Gavrikov, A., Knyazkov, D., and Aschemann, H. (2019). Heat transfer in cylindrical bodies controlled by a thermoelectric converter. *IFAC-PapersOnLine*, 52(15), 139–144.

Rauh, A., Kersten, J., and Aschemann, H. (2015). Experimental validation of LMI approaches for robust control design of a spatially three-dimensional heat transfer process. In *20th Int. Conf. MMAR-2015*, 11–16. IEEE, Miedzyzdroje.